Supramolecular Bionanocomposites 3: Effects of Surface Functionality on Electrical and Mechanical Percolation

Margaret J. Sobkowicz, Erick A. White, John R. Dorgan

Department of Chemical and Biochemical Engineering, Colorado School of Mines, Golden, Colorado 80401

Received 18 August 2010; accepted 26 February 2011
DOI 10.1002/app.34379
Published online 23 June 2011 in Wiley Online Library (wileyonlinelibrary.com).

ABSTRACT: Percolation phenomena in bionanocomposites composed of the bioplastic polylactide and surface decorated supramolecular multiwalled carbon nanotubes (MWCNTs) are investigated. MWCNTs with three distinct surface chemistries—a native surface, a hydroxyl functionalized surface, and a short hydrocarbon functionalized surface—are prepared and studied. Two experimental methods are used to determine percolation thresholds; melt rheology provides a measure of the mechanical percolation threshold and electrical impedance spectroscopy provides values of the electrical percolation threshold. The MWCNT-loading level required to obtain mechanical percolation is systematically found to be lower than the loading level needed to achieve electrical percolation. Hydroxylated MWCNTs have the highest percolation thresholds of 1.8 (mechanical) and 6.7 wt % (electrical), which is attributed to aggregation caused by hydrogen bonding. Alkane-grafted MWCNTs have lower percolation thresholds of 0.76 (mechanical) and 2.8 wt % (electrical). However, untreated MWCNTs have the lowest thresholds of 0.16 (mechanical) and 1.5 wt % (electrical). The reduced percolation threshold observed upon conversion of the hydroxylated surface to the alkylated surface is attributed to morphological differences—functionalization disrupts hydrogen bonding and leads to better nanotube dispersion. The combination of higher inherent conductivity and more favorable nanotube-polylactide interactions implies that unmodified MWCNTs are preferred to produce electrically conductive bionanocomposites. © 2011 Wiley Periodicals, Inc. J Appl Polym Sci 122: 2563–2572, 2011

Key words: carbon nanotubes; polylactide; electrical properties; thermomechanical properties; rheology

INTRODUCTION

Percolation phenomena are well known across a broad range of scientific fields. Examples include formal mathematical treatment in theoretical physics,[1] fluid transport in geophysics,[2] and various applications in materials science and engineering.[3] The percolation phenomenon may be described as a discontinuous or near discontinuous change in some measured property at a critical loading fraction (the percolation threshold) of a second phase.

Polymer composites with many types of fillers exhibit various percolation phenomena.[4] The critical volume fraction depends on aspect ratio, flexibility, and polydispersity of filler, the dispersion and alignment of filler in the matrix, and attractive or repulsive forces between filler particles and the polymer.[5] Electrical percolation also depends on the dielectric constant of the matrix material. Alignment of high-aspect-ratio particles results in an increase of the critical volume fraction due to reduced network connectivity.[6] Interactions between the filler and the polymer affect mechanical and electrical percolation differently. Fillers can influence the local viscosity at a distance on the order of the polymer molecular radius (tens of nm) from the surface of the particles. Electrical conductivity depends on much smaller atomic length scales than mechanical reinforcement. Although the exact mechanisms for electron transport in polymer composites are not fully understood, it is estimated that electrons cannot tunnel farther than 0.1 nm.[5] Both particle–polymer interactions and interparticle forces have important effects on mechanical load transfer.[7,8] Carbon nanotubes (CNTs) are particularly well suited for the comparison of mechanical and electrical percolation because of their high aspect ratio, modulus, and conductivity; however, other conductive fillers have been studied.[9,10]

CNTs have been targeted for polymer composite applications since their discovery almost two decades ago.[11] Composite modulus improvements of up

Correspondence to: M. Sobkowicz (sobko100@gmail.com).
Contract grant sponsor: Colorado Center for Biorefining and Biofuels, through the National Research Initiative Competitive Grant.
Contract grant sponsor: USDA Cooperative State Research, Education, and Extension Service; contract grant number: 2006-35504-16618.
Contract grant sponsor: National Science Foundation; contract grant number: CMMI-0700869.

to 1 TPa per volume percent loading have been shown as well as severalfold increases in strength.[12] Because of their unique mechanical,[13] electrical and chemical properties,[14] applications for polymer-CNT nanocomposites range from aeronautics, sensors, and drug delivery[15] to field emission and photovoltaic devices.[16,17]

Aggregation is still a major roadblock to the commercialization of CNT-polymer composites. Strategies for dispersion of nanoparticles include application of mechanical work (sonication or high shear mixing), chemical techniques (ionic or covalent surface modification), and combinations of the two.[18,19] Chemical modification gives the advantage of control over the interactions between the polymer matrix and the nanoparticle surface.[20] Effective load transfer to the CNTs requires not only a large surface area but also a strong adhesion force between the tubes and the matrix.[21,22] Chemical modification of the sidewalls often results in decreased CNT strength and electrical conductivity due to disruption of the π bonding structure.[23,24] Mechanical work can also damage CNTs, resulting in carbon debris and lower aspect ratio tubes.[25] Solution-based processing is convenient for aggregate breakup via sonication, while extrusion enables high-shear melt mixing.[26] Several novel approaches have also been described such as layer-by-layer assembly and self-assembly.[21,27] The literature thus demonstrates that preparation methodology has a large effect on nanocomposite properties.

In the present study, multiwalled carbon nanotubes (MWCNTs) are combined with polylactide (PLA) to produce novel electrically conductive nanocomposites having a biodegradable matrix. PLA is a renewable, biodegradable polymer commercially produced by catalytic polymerization of lactide monomers derived from renewable resources.[28] Researchers have incorporated many types of fillers into PLA in the recent years in attempts to improve the heat distortion temperature, gas barrier, crystallization kinetics, and mechanical properties.[29–32] Percolation properties of PLA composites have been investigated for layered silicate fillers[33] as well as CNTs.[34,35] Other rigid fillers such as cellulose nanowhiskers have been shown to percolate in other polymeric matrices.[27,36,37] Rheological and electrical spectroscopy studies have also been used as measures of enhanced dispersion in CNT nanocomposites.[7,38] Nanoparticle functionalization, which results in enhanced dispersion, can change the filler conductivity and insulate conductors from each other, further complicating the percolation picture.[9,39] Because of the complication of altered conductivity, complementary measurements of the mechanical percolation threshold can provide insight into nanocomposite structure. Finally, preparation techniques must be carefully controlled, because the degree of dispersion and alignment achieved influences the percolation threshold drastically.[8,40]

Supramolecular MWCNTs with three different surface chemistries (pristine, oxygenated, and alkane-grafted) are compared as nanofillers for producing PLA-based bionanocomposites. Electrical impedance spectroscopy and rheological measurements are used to determine and compare the electrical and mechanical percolation thresholds. The resulting supramolecular bionanocomposites possess the novel feature of combining electrical conductivity with a degradable matrix; such functionality provides great potential for the development of limited lifetime electronics, electrically active biomedical implants, and other novel devices.

MATERIALS AND METHODS

Chloroform, methanol, dodecylamine (DDA), *N*,*N*-dimethylformamide (DMF), and thionyl chloride from Sigma Aldrich were reagent grade and used as received. Multiwalled carbon nanotubes functionalized with hydroxyl groups (MWCNT-OH) and unfunctionalized MWCNT were obtained from CheapTubes.com. MWCNT-OH were 20–30 nm in diameter and 10–30 μm in length, as reported by the manufacturer. These dimensions correspond to aspect ratios varying from 333 to 1500. The MWCNT-OH were reported by the manufacturer as having 1.6 wt % OH functionality (0.011 mol fraction), surface area > 110 m^2/g, and electrical conductivity $>$ 100 S/cm. Before oxidation, the unfunctionalized MWCNT are identical to the MWCNT-OH. PLA 2000D grade (extrusion/thermoforming, MFI 4–8 g/10 min) was obtained from NatureWorks LLC and precrystallized at 80°C under vacuum for at least 14 h before use.

MWCNT-DDA were prepared using the acyl chloride reaction described in the literature.[41,42] MWCNT-OH were refluxed in thionyl chloride (3.33 mg/mL) with a small amount of DMF (1 mL per 30 mL thionyl chloride). After centrifuging 10 min at $8600 \times g$ and washing with chloroform, the MWCNT were added to melted DDA at a 10-fold stoichiometric excess relative to atomic carbon. The MWCNT were stirred in DDA 24 h, then diluted with chloroform, and centrifuged to remove unreacted DDA. The resulting MWCNT-DDA were washed repeatedly based on thermogravimetric analysis (TGA) measurements that indicated a fixed mass of grafted functionality (three times).

A solution blending technique was used to prepare all composites described in this work. A 10 wt % solution of PLA in chloroform was stirred overnight to ensure complete dissolution. Separately, 1 wt % suspensions ($\sim$ 15 mg/mL) of MWCNT,

MWCNT-OH, and MWCNT-DDA in chloroform were prepared using thoroughly dried carbon samples. The carbon suspensions were sonicated for 24 h and then added in appropriate ratios to the PLA solution to target dry compositions of 1, 4, 7, and 12 wt % (MWCNT and MWCNT-OH) and 0.5, 1, 2, 4, 7, and 12 wt % (MWCNT-DDA). Hereafter, composite samples are designated with a prefix denoting the nominal weight percent loading level and a suffix denoting the surface treatment (0.5MWCNT-PLA, 12MWCNT-DDA-PLA, etc). Solution-phase composites were stirred on magnetic stir plates for 48 h and then precipitated into 10-fold excess methanol as a means of preventing nanoparticle aggregation. Precipitate was collected, dried overnight, and further dried under vacuum (25 in Hg) at 60°C for at least 24 h.

Melt rheology

Nanocomposite samples were prepared for rheological testing using a previously developed protocol.[43–45] Composite samples were dissolved in chloroform at a concentration of 3 wt %. Tris(nonyl phenyl) phosphine solution was added at a level of 0.5 wt % (relative to composite mass) as a melt stabilizer. Composite solutions were stirred for 24 h and cast onto glass plates. Once the solvent was evaporated, films were vacuum dried for 48 h at 80°C, 25 in Hg. Films were then cut up and vacuum/compression molded into circular discs (2 mm thick × 8 mm diameter) and crystallized at 110°C for 3 h. Rheological measurements were made in the melt at 175°C using a Rheometrics ARES-LS rheometer with 8-mm parallel plate fixtures. Strain sweeps were performed to determine the limits of linear viscoelasticity; all subsequent testing was performed within the linear region.

Electrical impedance spectroscopy

Electrical impedance spectra were collected using a Gamry PCI4/300 potentiostat. About 8-mm silver/silver chloride electrodes (In Vivo Metric, Healdsburg, CA) were fixed to either side of a 3 mm × 12 mm × 45 mm compression-molded test bar, prepared freshly from the solution-blended film samples described earlier, using colloidal silver paste (Electron Microscopy Sciences, Hatfield, PA). The paste was allowed to dry for at least 4 h to ensure repeatability through complete evaporation of the solvent carrier. Frequency was varied from 10^{-2} Hz to 10^5 Hz using a 100-mV root-mean-squared amplitude perturbation. Specific admittance (C_{sp}) curves were calculated according to eq. (1) using the impedance modulus ($|Z|$) and the sample and electrode geometry; $l = 0.3$ cm is sample thickness and $r = 0.4$ cm is electrode radius.

$$C_{sp} = \frac{l}{|Z|\pi r^2} \quad (1)$$

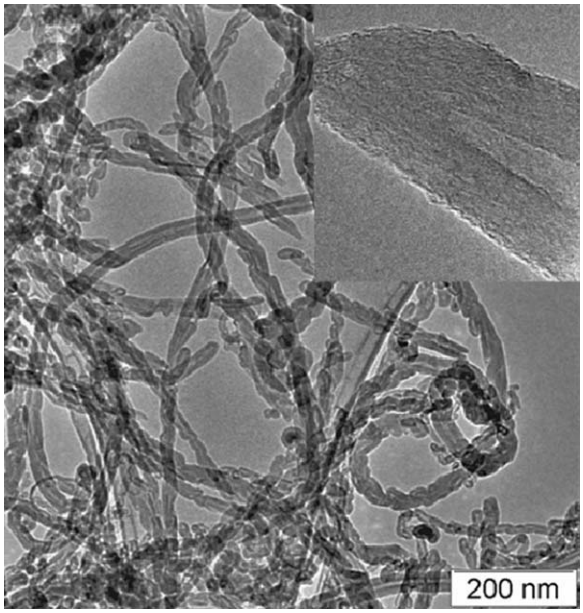

Figure 1 TEM image of MWCNT-OH. Inset: close-up view of graphitic sidewalls.

Optical microscopy

Thin-film samples of the 1MWCNT, 2MWCNT-OH, and 2MWCNT-DDA compression-molded bars from impedance spectroscopy tests were prepared for optical microscopy. Samples of 13 ± 1 mg were melted onto glass slides on a hot plate. Coverslips were pressed into the melted polymer to form disks about 1.5 cm in diameter and about 60 μm in thickness. They were cooled rapidly to room temperature and examined at 10× and 40× magnification.

RESULTS AND DISCUSSION

A TEM image of MWCNT-OH is shown in Figure 1. The CNT have an entangled network structure, and the inset shows the graphitic structure of the tube walls. The thermal stability of the materials and the amount of functionalization achieved is detailed in Ref. 32. It was found that the MWCNT-DDA have 0.7 mol % DDA groups per mol carbon. This is equivalent to 3 groups/nm^2 when using the manufacturer-reported surface area value of 110 m^2/g.

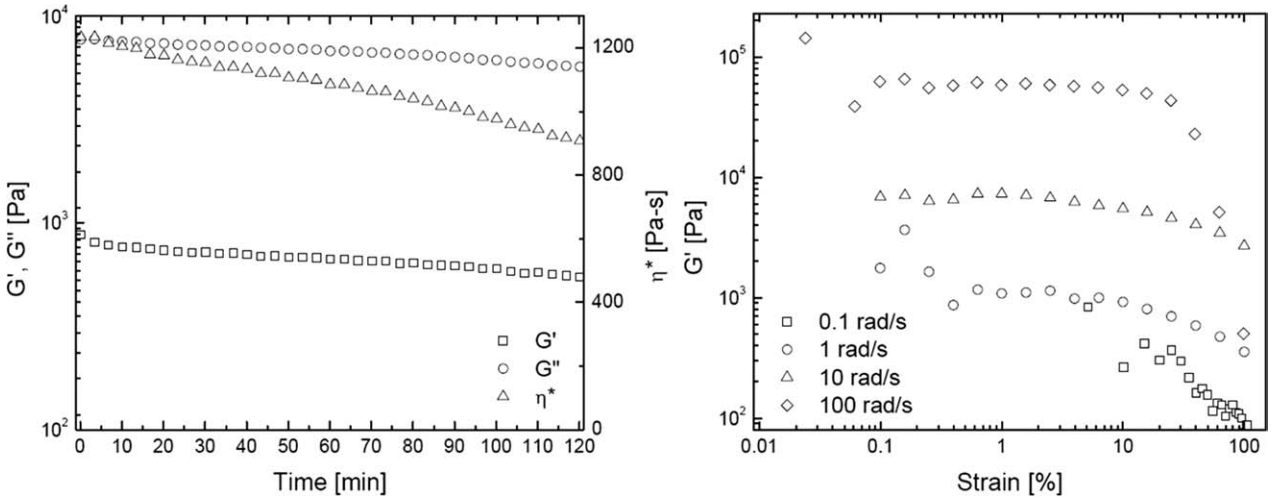

Figure 2 (a) Time sweep test at 1 Hz for TNPP-stabilized pure PLA at 175°C. (b) Strain sweeps at different frequencies for 2MWCNT-PLA demonstrating limits of linear viscoelasticity in the bionanocomposites.

Melt rheology

The melt stability of the materials is demonstrated in Figure 2(a), which shows that over an hour of testing at 175°C the viscosity decreases by only 12%. This is consistent with previous studies.[45] A similar decrease is evident in the loss modulus, G'', which dominates the viscoelastic response at the testing temperature. The decreases in viscosity and modulus are projected to be smaller in the composites due to the increased thermal stability of CNT-polymer composites.[46] Accordingly, all samples were tested within one hour of heating to 175°C.

For oscillatory testing, the strain values were selected based on the results of the strain sweeps shown in Figure 2(b). For all but the highest frequency, the moduli are constant over the range from 0.5 to 5% strain. At the lowest strains, modulus values are scattered due to operating at the lower end of the dynamic range of the torque transducer. Appropriate strains are selected to be large enough to provide sufficient transducer signal but small enough to remain in the linear regime. Plots of storage modulus (G') as a function of frequency (ω) are shown in Figure 3 for the various surface-treated nanotubes at different loading levels. Slopes of the $G'(\omega)$ and $G''(\omega)$ (not shown) logarithmic plots for unfilled PLA are 2 and 1, as expected in the terminal regime.[47] For all bionanocomposites, the storage modulus becomes independent of frequency at higher loading levels, indicating a transition to solid-like behavior. This transition is less dramatic for the MWCNT-OH. For the highest weight loading, 13MWCNT-OH, the storage modulus is an order of magnitude lower than that of the 13MWCNT and 13MWCNT-DDA.

Complex viscosities are plotted versus frequency in Figure 4. Because the MWCNTs are curved and tangled into a weblike structure, it is anticipated that the full length of the tubes does not necessarily participate in the stress transfer. Rather, there is some characteristic persistence length associated with the specific level of dispersion achieved and it is this persistence length that affects the modulus and viscosity of the melt. The Maron–Pierce equation has been used to describe the viscosity of suspensions[47]:

$$\eta_r = \frac{\eta}{\eta_0} = \frac{1}{[1 - \phi/A]^2} \tag{2}$$

where η_0 is the viscosity of the suspending fluid, η is the viscosity of the suspension, ϕ is the volume fraction of particles, and A is a fitting parameter that has empirically been found to be close to the maximum packing fraction of the suspended particles. Volume fractions were determined using a density of 1.9 g/cm^3 for the MWCNT, this density was calculated based on average tube dimensions. Higher aspect ratio fillers have lower values for A. The viscosity data at an intermediate value, 1 Hz, are applied to eq. (2), and the values for A are given in Table I. Figure 5 shows the linear plot of $\eta_r^{-1/2}$ at 1 Hz versus MWCNT volume fraction and the fits from which A values were derived. Although there is a lot of scatter in the data (R^2 values for the linear fits are 0.76, 0.95, and 0.88 for MWCNT, MWCNT-OH, and MWCNT-DDA, respectively), it is clear that the viscosity of the melts is higher at lower loading levels for the MWCNT-DDA composites than for the MWCNT-OH composites. Positive deviation from linearity at the highest volume fractions in MWCNT and MWCNT-DDA composites leads to less negative slopes and higher A values, likely due to polydispersity in particle size.[47] The lowest A for MWCNT-DDA indicates a higher effective aspect ratio in these

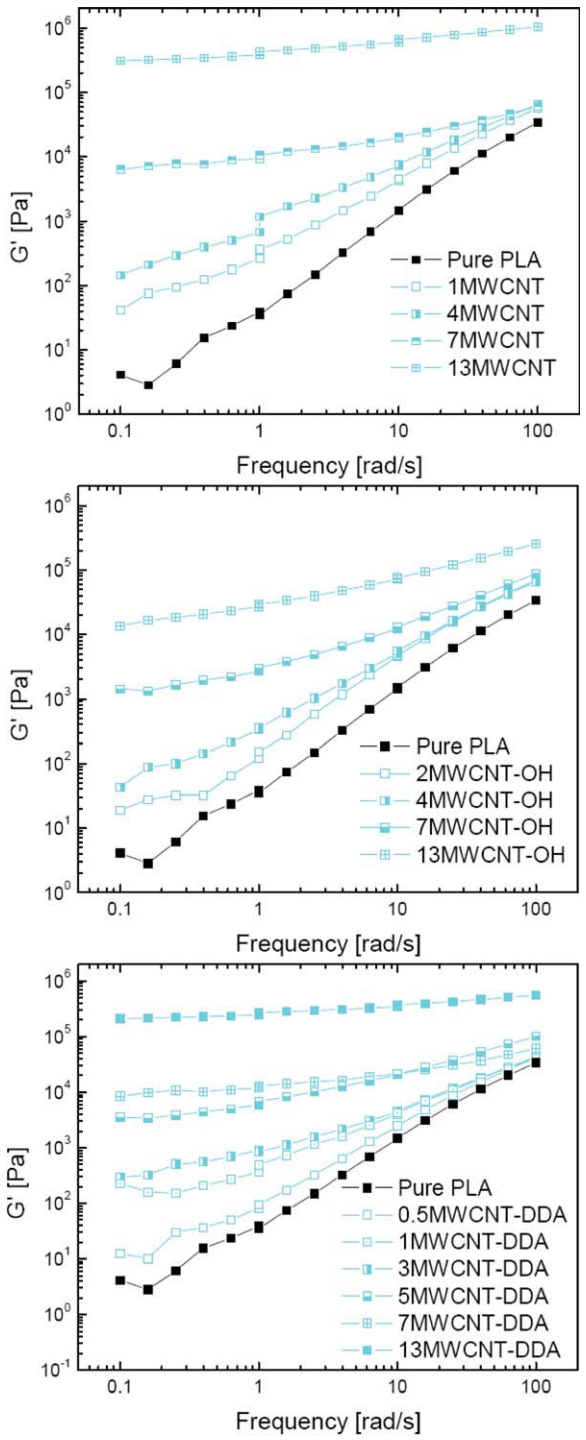

Figure 3 Storage modulus for (top) MWCNT composites (middle) MWCNT-OH composites and (bottom) MWCNT-DDA composites from melt rheology. [Color figure can be viewed in the online issue, which is available at wileyonlinelibrary.com.]

composites. Evidence of enhanced dispersion based on crystallization kinetics was found for DDA-functionalized carbon in earlier work.[32] It is unclear how the surface functionality affects specific interactions between the polymer chains and the nanotube surface; however, because the effects of dispersion and surface interaction cannot be easily decoupled.

To pinpoint the mechanical percolation more precisely, G' at 1 Hz is plotted versus weight loading in Figure 6. A mechanical percolation model analogous to that commonly used for electrical percolation is employed to interpret the data.[36,48]

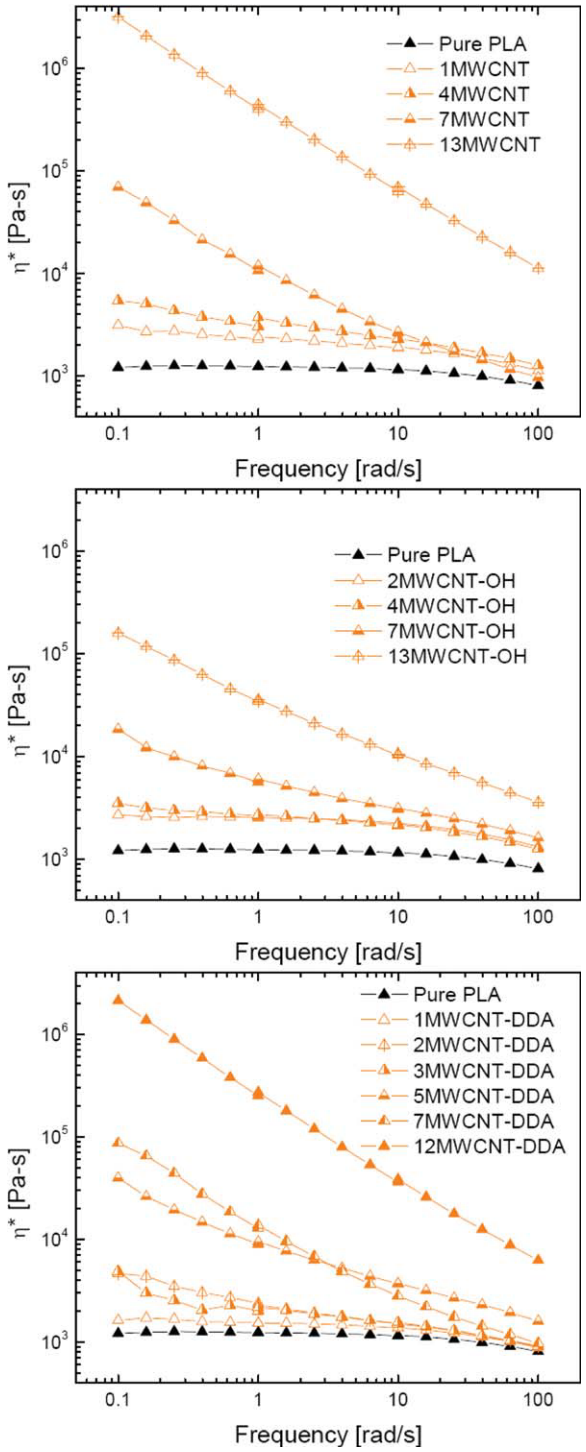

Figure 4 Complex viscosity versus frequency for all composites. [Color figure can be viewed in the online issue, which is available at wileyonlinelibrary.com.]

TABLE I
Summary of Mechanical and Electrical Percolation Parameters Determined for All Filler Types

	Modulus properties @ $w = 1$ Hz			Conductivity properties @ $w = 0.01$ Hz		
Filler type	A	w_c	t	C_f (S/cm)	w_c	t
MWCNT	0.087	0.0015	1.8	80	0.015	2.3
MWCNT-OH	0.099	0.018	2.6	2	0.067	2.3
MWCNT-DDA	0.077	0.012	1.8	0.5	0.028	2.3

$$G_c = \frac{(1 - 2\psi + \psi w)G_p G_f + (1 - w)\psi G_f^2}{(1 - \psi)G_f + (w - \psi)G_p},$$
$$\psi = G_f \left[\frac{w - w_c}{1 - w_c}\right]^t \quad (3)$$

In eq. (3), G_c is the shear modulus of the composite, G_f is the shear modulus of the pure filler material, G_p is the modulus of the pure polymer, w is the filler weight fraction, and w_c is the critical weight fraction for percolation. The exponent t is a universal network scaling parameter found by deGennes to have a theoretical value of 1.8 for networks when network-dangling ends are included.[49] Shear storage modulus values for MWCNT have been found by theory and experiment to be on the order of 100 GPa, but it has also been shown that, due to the curved structure of MWCNT maintained in composites, the effective value is reduced by several orders of magnitude.[50] The value best describing the data in Figure 6 was 0.2 GPa. Critical weight-loading values are also found in Table I; the masses correspond to volume fractions of 0.001 (MWCNT), 0.012 (MWCNT-OH), and 0.008 (MWCNT-DDA). To make a reasonable fit with the MWCNT-OH data, a percolation exponent of 2.6 had to be used. The other two curves use a value of 1.8, as theory predicts. The higher exponent found for MWCNT-OH is an indication that less of the MWCNT-OH mass contributes to the mechanical percolation due to aggregation of the tubes. Interestingly, it appears that although the MWCNT-DDA has a lower A value and therefore longer persistence length, this does not necessarily translate to lower weight loading for percolation. Other factors such as interactions of the polymer chains with the surface of the MWCNT can contribute, and it may be that the DDA chains on the surface of the tubes act as a surfactant, keeping viscosity, and modulus values lower even though dispersion is improved. Previous work[32] shows that T_g is unchanged in these composites, as measured by both differential scanning calorimetry and mechanical spectroscopy, likely due to competing effects of plasticization and chain confinement on the nanosurface.

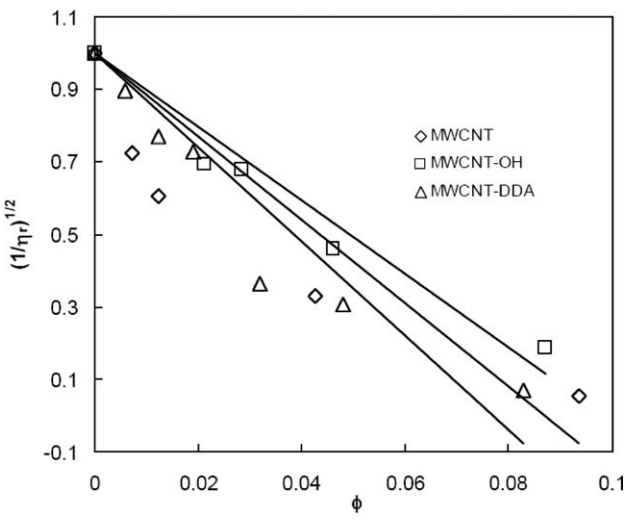

Figure 5 Linear fits to the Maron–Pierce equation for suspension viscosity.

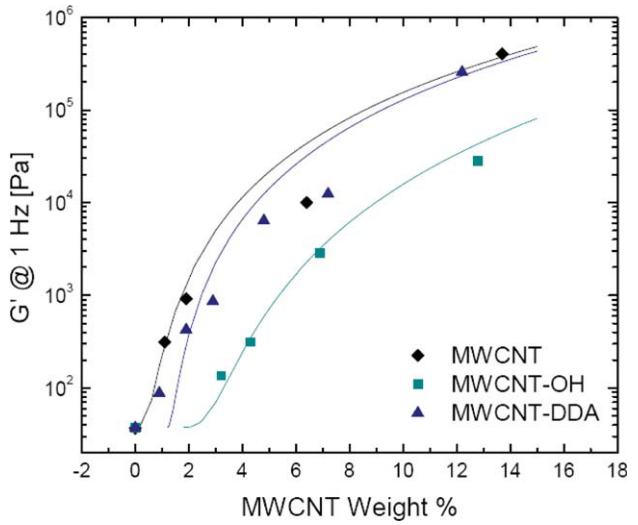

Figure 6 Storage modulus at 1 Hz versus weight loading for all composites. Fitted curves represent eq. (3). [Color figure can be viewed in the online issue, which is available at wileyonlinelibrary.com.]

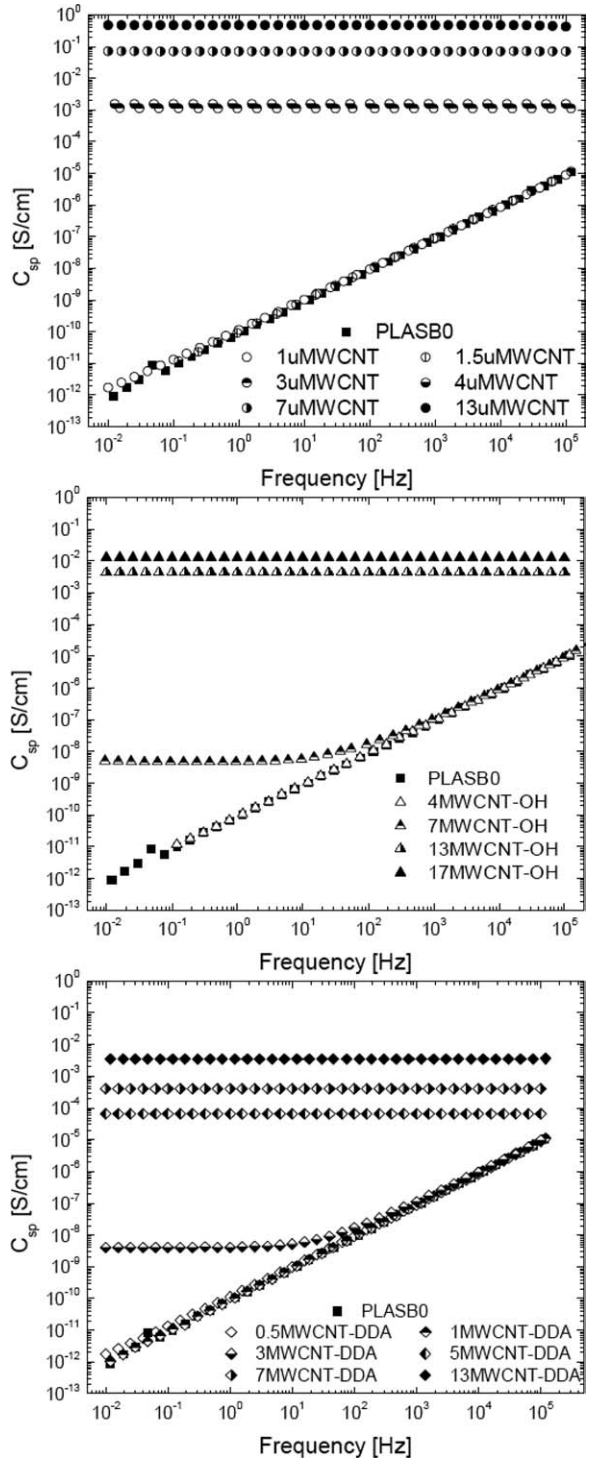

Figure 7 Electrical impedance spectroscopy data for all composites.

Electrical impedance spectroscopy

Specific admittance data are plotted versus frequency in Figure 7. In the case of MWCNT-OH, an additional weight loading was prepared and tested (17MWCNT-OH) because of the high-critical weight fraction needed to obtain percolation for these hydroxylated surfaces. In the case of MWCNT, 1.5 and 3 wt % samples were prepared and tested to provide additional data near the percolation threshold; this enables a more precise determination of the exact threshold. The data for nonconductive samples coincides almost exactly with the pure PLA data, whereas conducting samples have a specific admittance independent of frequency. Samples just beginning to percolate show a transition from frequency-independent conductivity at low frequencies to nonconductive behavior at higher frequencies.

Figure 8 shows the low-frequency limit admittance (DC conductivity) versus weight loading for MWCNT, MWCNT-OH, and MWCNT-DDA. Percolation thresholds were determined by fitting the data in Figure 8 to eq. (4)[51,52]

$$C_{\mathrm{sp}} = C_f \left[\frac{w - w_c}{1 - w_c}\right]^t \tag{4}$$

where C_f is the pure filler conductivity, w is the composite weight loading, w_c is the critical weight fraction, and t is the critical exponent. Fitting parameters are listed in Table I. Pure filler conductivities were estimated to be 80 S/cm for MWCNT, 2 S/cm for MWCNT-OH, and 0.5 S/cm for MWCNT-DDA. The MWCNT value agrees well with the manufacturer-reported value; however, surface functionalization significantly reduced the conductivity. This is likely due to disruption of the π bonding during covalent modification as well as insulation from the presence of the encapsulating grafted organic moiety. The percolation exponent for all three materials was determined to be close to the theoretical value of 2 for a three-dimensional lattice. Critical weight fractions were found to be 0.015 for MWCNT, 0.028

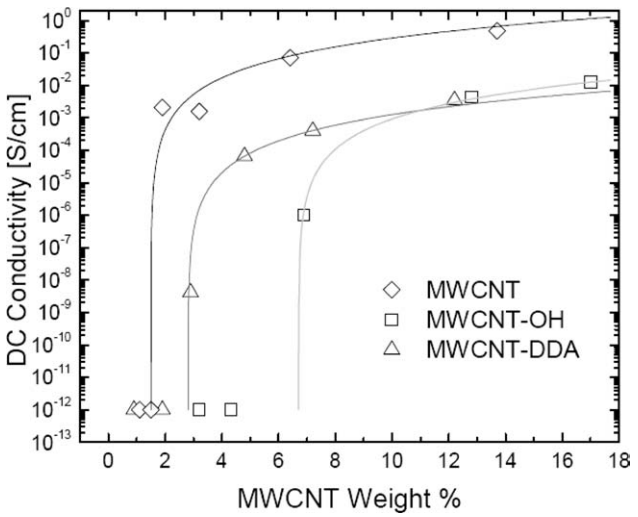

Figure 8 DC conductivity from low frequency impedance data versus weight fraction carbon in PLA composites. Lines are fits to the data based on eq. (4).

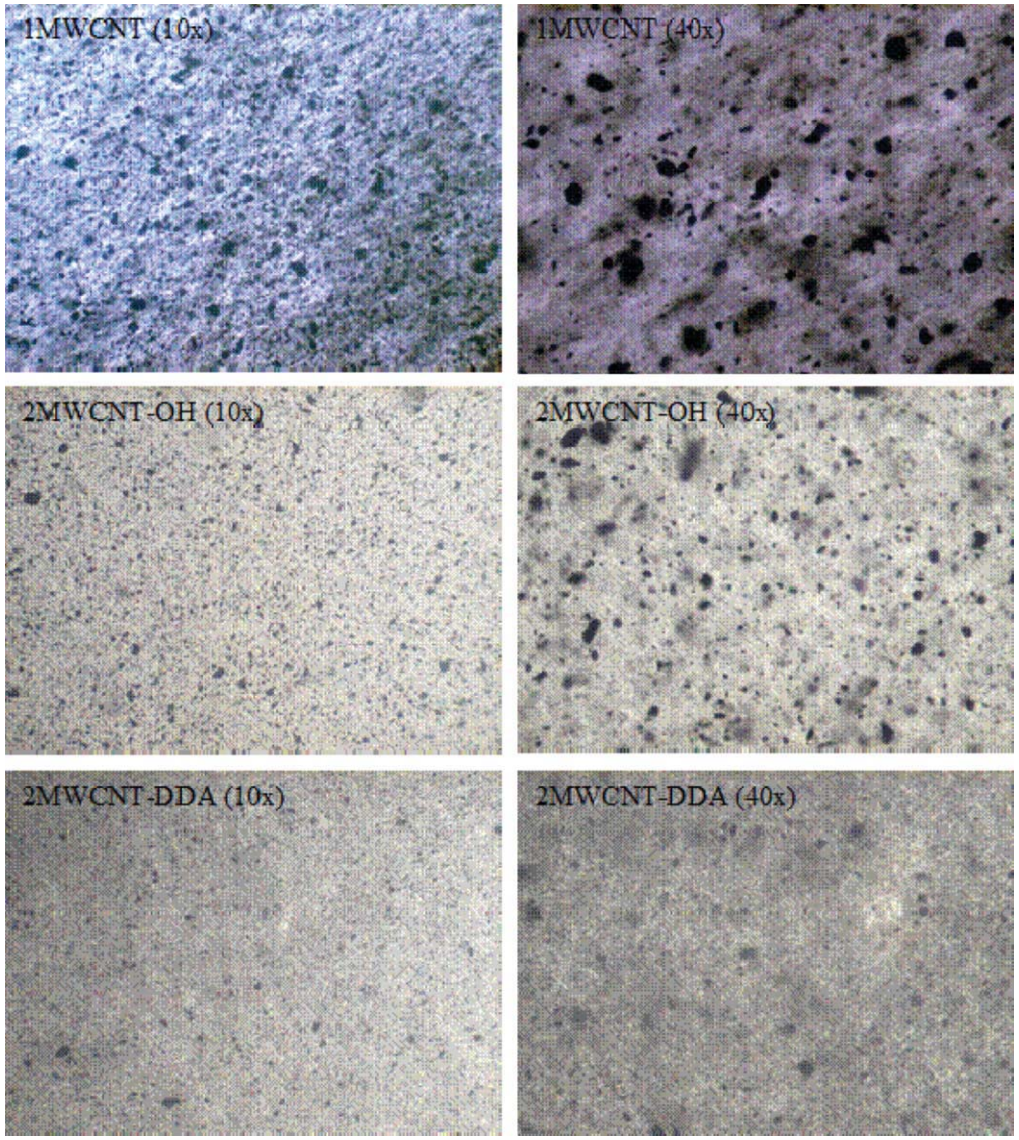

Figure 9 Optical micrographs of lower weight loading composites at two magnifications. Images were taken near the same spot for each magnification and white balance was adjusted to give equal contrast for each sample. [Color figure can be viewed in the online issue, which is available at wileyonlinelibrary.com.]

for MWCNT-DDA, and 0.067 for MWCNT-OH. These weight loadings correspond to volume fractions of 0.0099, 0.0190, and 0.0450, respectively. The MWCNT-DDA form a conducting network at a value slightly higher than that of the MWCNT but the MWCNT-OH require much more material; they are much less effective in achieving both electrical and mechanic percolation. In all cases, the electrical percolation thresholds are higher than those found for the mechanical percolation. This result is expected, because electrons cannot hop very far in the insulating polymer, that is, the tubes must be extremely close to allow electron transport. MWCNTs before functionalization have the best percolation properties, MWCNT-DDA perform almost as well, while the MWCNT-OH is far less effective. This is likely due to hydrogen bonding, which causes the MWCNT-OH to aggregate and interact less favorably with the PLA matrix. Interestingly, the electrical and mechanical percolation thresholds are fairly close for the MWCNT-DDA, which may have important implications when improvements in both properties are design targets. Theoretical volume fractions for percolation of randomly oriented, high-aspect-ratio, rigid rods are reported to be on the order of the inverse of the aspect ratio: $\phi_c \propto D/L$ for $L/D \gg 1$.[5,6,53] The manufacturer-reported aspect ratio for the MWCNT ranges from 333 to 1500, which corresponds to a theoretical critical volume fraction of 0.001–0.002. Comparing the critical percolation thresholds found here for the curved, flexible MWCNT, effective aspect ratios of the nanotube

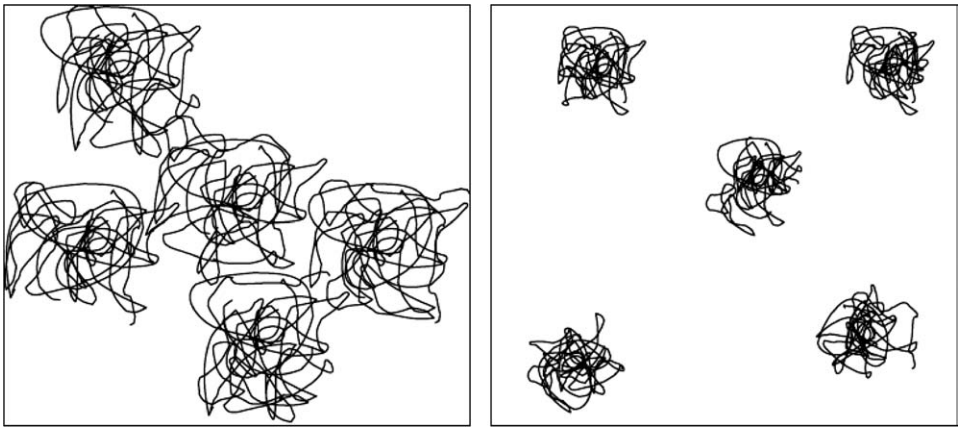

Figure 10 Schematic representation of equal-mass systems for (left) looser, percolated aggregates and (right) tighter, isolated aggregates.

networks are determined to be 101, 52, and 22 for MWCNT, MWCNT-DDA, and MWCNT-OH, respectively.

The alkylated MWCNT exhibit lower percolation thresholds than the hydroxylated tubes from which they are derived; however, the weight fraction for percolation does not drop below that of the untreated tubes. To understand this phenomenon, microscopy images showing the morphology of 1MWCNT, 2MWCNT-OH, and 1MWCNT-DDA composites are shown in Figure 9. All three types of tubes appear reasonably well distributed, but the MWCNT composites have significantly larger aggregates than either MWCNT-OH or MWCNT-DDA. There also appears to be a larger visible fraction of carbon in the MWCNT sample; this is likely due to limits of detection at only 400× magnification. For the MWCNT-DDA, even at the higher magnification, no really large aggregates are visible. There instead appears to be a darker background in the image, indicating that nanotubes are better dispersed, and the clusters are not individually resolvable. Signs of poor dispersion were also seen in cast films of the three composites. The MWCNT had a rough texture with islands visible in the film, whereas both the MWCNT-OH and MWCNT-DDA composite films appeared more uniform and smooth to the touch.

The low percolation of the MWCNT composites can be explained through classical dispersion and distribution arguments. It is possible that large-scale aggregates of tubes can percolate at a lower volume fraction than well distributed—but isolated—smaller aggregates. This is drawn schematically in Figure 10. The first case has larger, less dense aggregates that can connect from one end of the material to the other. The second has smaller aggregates that are more compact, and no connectivity is exhibited. Because of hydrogen bonding, the MWCNT-OH likely form tighter, denser aggregates. The DDA functionalization disrupts this aggregation leading to larger, less dense aggregates.

CONCLUSIONS

Three different types of MWCNT were shown to have differing percolation thresholds when solution blended with PLA to form novel supramolecular conductive bionanocomposites. Mechanical percolation thresholds were lower than electrical thresholds for all types of MWCNT; however, the two thresholds were closest in value for MWCNT-DDA. The MWCNT-OH had significantly higher thresholds than the other two fillers; poor dispersion due to hydrogen bonding is likely responsible for the higher threshold. The MWCNTs have the lowest critical weight fraction for both types of percolation; this is likely due in part to the higher material strength and conductivity for the undisrupted π-bonding structure of the unfunctionalized surface and also to the looser structure of aggregates.

The relationship between electrical and mechanical properties in polymer composites is complex, and interfacial properties have an effect on both dispersion and electrical or mechanical load transfer throughout these two-phase materials. Both surface functionalities result in less conductive materials overall, but threshold loading is lower when aggregate morphology is looser and more entangled, as it appears to be for untreated or alkylated surfaces. This picture is further complicated for mechanical properties, because the grafted functionality may lower the polymer viscosity, while larger aggregates may introduce defects that lower composite impact resistance. There is an inherent tradeoff between nanotube electrical and mechanical properties and the desired composite morphology. Clearly, the intended application must be carefully considered when deciding upon a property window enabled by

choosing a surface functionality in electrically conductive supramolecular bionancomposites.

References

1. Kirkpatrick, S. Rev Mod Phys 1973, 45, 574.
2. Berkowitz, B. Math Geol 2005, 27, 467.
3. Xie, P.; Gu, P.; Beaudoin, J. J. J Mater Sci 1996, 31, 4093.
4. Stauffer, D.; Aharony, A. Introduction to Percolation Theory; Taylor & Francis: London, 1992.
5. Kyrylyuk, A. V.; van der Schoot, P. Proc Natl Acad Sci 2008, 105, 8221.
6. Celzard, A.; McRae, E.; Deleuze, C.; Dufort, M.; Furdin, G.; Mareche, J. F. Phys Rev B 1995, 53, 6209.
7. Potschke, P.; Abdel-Goad, M.; Alig, I.; Dudkin, S.; Lellinger, D. Polymer 2004, 45, 8863.
8. Du, F.; Scogna, R. C.; Zhou, W.; Brand, S.; Fishcher, J. E.; Winey, K. I. Macromolecules 2004, 37, 9048.
9. Gelves, G. A.; Lin, B.; Sundararaj, U.; Haber, J. A. Nanotechnology 2008, 19, 215712.
10. Roldughin, V. I.; Vysotskii, V. V. Prog Org Coat 2000, 39, 81.
11. Ajayan, P. M.; Tour, J. M. Nature 2007, 447, 1066.
12. Coleman, J. N.; Khan, U.; Blau, W. J.; Gun'ko, Y. K. Carbon 2006, 44, 1624.
13. Coleman, J. N.; Khan, U.; Gun'ko, Y. K. Adv Mater 2006, 18, 689.
14. Niyogi, S.; Hamon, M. A.; Hu, H.; Zhao, B.; Bhowmik, P.; Sen, R.; Itkis, M. E.; Haddon, R. C. Acc Chem Res 2002, 35, 1105.
15. Prato, M.; Kostarelos, K.; Bianco, A. Acc Chem Res 2007, 41, 60.
16. Dresselhaus, M. S.; Dresselhaus, G.; Avouris, P. Carbon Nanotubes: Synthesis, Structure, Properties and Applications; Springer-Verlag: Berlin, Germany, 2001.
17. Breuer, O.; Sundararaj, U. Polym Compos 2004, 25, 630.
18. Xie, X.-L.; Mai, Y.-W.; Zhou, X.-P. Mater Sci Eng R 2005, 49, 89.
19. Sun, Y.-P.; Fu, K.; Lin, Y.; Huang, W. Acc Chem Res 2002, 35, 1096.
20. Tasis, D.; Tagmatarchis, N.; Bianco, A.; Prato, M. Chem Rev 2006, 106, 1105.
21. Moniruzzaman, M.; Winey, K. I. Macromolecules 2006, 39, 5194.
22. Ajayan, P. M.; Schadler, L. S.; Giannaris, C.; Rubio, A. Adv Mater 2000, 12, 750.
23. Andrews, R.; Weisenberger, M. C. Curr Opin Solid State Mater Sci 2003, 8, 31.
24. Wang, C.; Guo, Z.-X.; Fu, S.; Wu, W.; Zhu, D. Prog Polym Sci 2004, 29, 1079.
25. Badaire, S.; Poulin, P.; Maugey, M.; Zakri, C. Langmuir 2004, 20, 10367.
26. Krishnamoorti, R.; Vaia, R. A. Polymer Nanocomposites; Oxford University Press: San Francisco, CA, 2000.
27. Capadona, J. R.; Van Den Berg, O.; Capadona, L. A.; Schroeter, M.; Rowan, S. J.; Tyler, D. J.; Weder, C. Nat Nanotechnol 2007, 2, 765.
28. Hartmann, M. H. In Biopolymers from Renewable Resources; Kaplan, D. L., Ed.; Springer: New York, 1998.
29. Ray, S. S.; Yamada, K.; Okamoto, M.; Fujimoto, Y.; Ogami, A.; Ueda, K. Polymer 2003, 44, 6633.
30. Braun, B.; Dorgan, J. R.; Knauss, D. M. J Polym Environ 2006, 14, 49.
31. Sobkowicz, M. J.; Dorgan, J. R.; Gneshin, K. W.; Herring, A. M.; McKinnon, J. T. J Polym Environ 2008, 16, 131.
32. Sobkowicz, M. J.; Sosa, R.; Dorgan, J. R. J Appl Polym Sci 2011, 121: n/a. doi:10.1002/app.33787.
33. Pluta, M.; Jeszka, J. K.; Boiteuz, G. Eur Polym J 2007, 43, 2819.
34. Tsuji, H.; Kawashima, Y.; Takikawa, H.; Tanaka, S. Polymer 2007, 48, 4213.
35. Kim, H.-S.; Park, B. H.; Yoon, J.-S.; Jin, H.-J. Eur Polym J 2007, 43, 1729.
36. Favier, V.; Canova, G. R.; Shrivastava, S. C.; Cavaille, J. Y. Polym Eng Sci 1997, 37, 1732.
37. Flandin, L.; Brechet, Y.; Cavaille, J. Y. Compos Sci Technol 2000, 61, 895.
38. Kodgire, P. V.; Bhattacharyya, A. R.; Bose, S.; Gupta, N.; Kulkarni, A. R.; Misra, A. Chem Phys Lett 2006, 432, 480.
39. Masenelli-Varlot, K.; Chazeau, L.; Gauthier, C.; Bogner, A.; Cavaille, J. Y. Compos Sci Technol 2009, 69, 1533.
40. Sandler, J. K. W.; Kirk, J. E.; Kinloch, I. A.; Shaffer, M. S. P.; Windle, A. H. Polymer 2003, 44, 5893.
41. Chen, J.; Hamon, M. A.; Hu, H.; Chen, Y.; Rao, A.; Eklund, P. C.; Haddon, R. C. Science 1998, 282, 95.
42. Sobkowicz, M. J.; Dorgan, J. R.; Gneshin, K. W.; Herring, A. M.; McKinnon, J. T. Carbon 2008, 47, 622.
43. Lehermeier, H. J.; Dorgan, J. R. Polym Eng Sci 2001, 41, 2172.
44. Dorgan, J. R.; Janzen, J.; Clayton, M. P.; Hait, S. B.; Knauss, D. M. J Rheol 2005, 49, 607.
45. Palade, L.-I.; Lehermeier Hans J.; Dorgan, J. R. Macromolecules 2001, 34, 1384.
46. Biercuk, M. J.; Llaguno, M. C.; Radosavljevic, M.; Hyun, J. K.; Johnson, A. T. Appl Phys Lett 2002, 80, 2767.
47. Dealy, J. M.; Wissbrun, K. F. Melt Rheology and Its Role in Plastics Processing; Kluwer Academic: Boston/Dordrecht, 1999.
48. Dalmas, F.; Cavaille, J. Y.; Gauthier, C.; Chazeau, L.; Dendievel, R. Compos Sci Technol 2006, 67, 829.
49. de Gennes, P.-G. Scaling Concepts in Polymer Physics; Cornell University Press: Ithaca, NY, 1979.
50. Fisher, F. T.; Bradshaw, R. D.; Brinson, L. C. Compos Sci Technol 2003, 63, 1689.
51. Kluppel, M. Adv Polym Sci 2003, 164, 1.
52. Alig, I.; Skipa, T.; Lellinger, D.; Bierdel, M.; Meyer, H. Phys Status Solidi B 2008, 245, 2264.
53. Balberg, I.; Anderson, C. H.; Alexander, S.; Wagner, N. Phys Rev B 1984, 30: 3933.